Subsonic Flutter of Panels on Continuous Elastic Foundations

JOHN DUGUNDJI,* EARL DOWELL,† AND BRIAN PERKIN‡
Massachusetts Institute of Technology, Cambridge, Mass.

The subsonic aeroelastic stability of a two-dimensional panel resting on a continuous elastic foundation was investigated. Tests were conducted experimentally on a 104- × 24- × 0.018-in. rectangular aluminum panel in a low-speed wind tunnel. Definite flutter of a traveling-wave-type was observed. Films and oscillograph records were taken. Theoretically, a finite-panel, two-mode, standing-wave analysis was shown to give essentially the same behavior as the infinite-panel, traveling-wave analysis of Miles for this panel. Although a mild, divergence-type instability exists for these panels, the principal instability was shown to be of a traveling-wave, flutter-type. Comparison of experiment and theory showed good agreement in flutter speed and wavelength but poor agreement in wave speed and frequency at flutter. This discrepancy was attributed to limitations in the test set-up as well as to the general difficulty of predicting the wave speed and frequency as accurately as the flutter speed. The present investigation should be of interest in problems of hydroelasticity, axially symmetric cylinders, and inflatable structures at low speeds, as well as to panels lying on springy elastic materials.

Nomenclature

A = amplification factor (infinite panel)
$\bar{A}$ = amplification factor (finite panel)
A_0, A_2, A_4 = constants
B = damping constant
c = wave speed relative to air at rest
$c + U$ = wave speed relative to panel
c_0 = wave speed in vacuum
D = $Eh^3/12(1 - \nu^2)$ = plate flexural rigidity
(DR) = damping ratio
E = modulus of elasticity
f_1 = correction factor given by Eq. (16)
f_2 = mode factor given by Eq. (39)
G = $B\lambda/2\pi mU$ = nondimensional damping
h = plate thickness
i = $(-1)^{1/2}$
K = spring stiffness of elastic foundation
$\bar{K}$ = Kl^4/D = nondimensional spring stiffness parameter
l = length of panel
m = mass of panel per unit area
n = mode number
p = pressure
p_∞ = pressure of air at freestream
q_n = generalized coordinate
Q = $\rho_\infty U^2 l^3/D$ = nondimensional dynamic pressure parameter
s = root of characteristic equation (actual time)
$\bar{s}$ = $s/[D/ml^4]^{1/2}$ = root of characteristic equation (nondimensional time)
t = time
$\bar{t}$ = $t[D/ml^4]^{1/2}$ = nondimensional time
U = air speed at freestream
w = deflection of plate
x = coordinate
Δp = differential pressure loading over panel = $p_L - p_U$
ζ = c/U
ζ_0 = c_0/U
λ = wavelength
μ = $\rho_\infty \lambda/m2\pi$ = mass density ratio (infinite panel)
$\bar{\mu}$ = $\rho_\infty l/m\pi$ = mass density ratio (finite panel)
ν = Poisson's ratio
ξ = coordinate
ρ_∞ = density of air at freestream
ϕ_n = nth free vibration mode
ω = frequency

Presented at the IAS 31st Annual Meeting, New York, January 21–23, 1963; revision received March 11, 1963. This work was supported by the Air Force Office of Scientific Research under Contract No. AF 49(638)-219.

* Associate Professor of Aeronautics and Astronautics. Member AIAA.
† Research Assistant, Department of Aeronautics and Astronautics. Member AIAA.
‡ Engineer, Blackburn Aircraft Company, England.

1. Introduction

THE problem considered here is the aeroelastic stability of a long panel resting on a continuous elastic foundation. Such a situation might arise for a panel lying on some springy insulating material exposed to an air flow over its top side.

The theory of Miles[1] for infinitely long panels can be adapted readily to describe this behavior. In this theory, unstable traveling waves are predicted above a critical flutter speed for both the subsonic and supersonic cases. For panels resting on an elastic foundation, these unstable traveling waves possess a finite wavelength and hence give the possibility of actually viewing these waves on a long panel. Accordingly, it was decided to build such a panel and test it in a conveniently available low-speed wind tunnel. It was hoped to shed some light on the traveling wave vs standing wave theories of panel flutter both experimentally and theoretically and also to reinvestigate the possibility of panel flutter at subsonic speeds.

The present article is a condensed version of a previous report on the subject by the authors.[2] Some earlier preliminary work in this general area was done by Dowell.[3]

2. Experiment

a. Panel Test Model

The model to be tested consisted basically of a flat rectangular sheet of aluminum 2024-T3 with dimensions§ 104 × 24 × 0.018 in. The panel was orthogonally stiffened by a series of aluminum angle stiffeners, spaced 1.58 in. apart and running perpendicular to the long edges of the panel. The panel was attached to a rigid wooden box frame by resting on three rows of helical springs running parallel to the long edges of the panel and by a mylar strip hinge along the leading edge of the panel. The two long edges of the panel were left free, whereas the trailing edge was left free during some of the tests and pinned down during others. A sketch of the panel and its support system is shown in Fig. 1.

The aluminum angle stiffeners and the helical coil springs were attached to the aluminum sheet by Armstrong A-2 epoxy resin glue. The angle stiffeners were used to insure two-di-

§ Early in the test program (run 17), the very rear part of the panel was damaged. The panel then was shortened from 104 in. to 93 in. for the remainder of the tests.

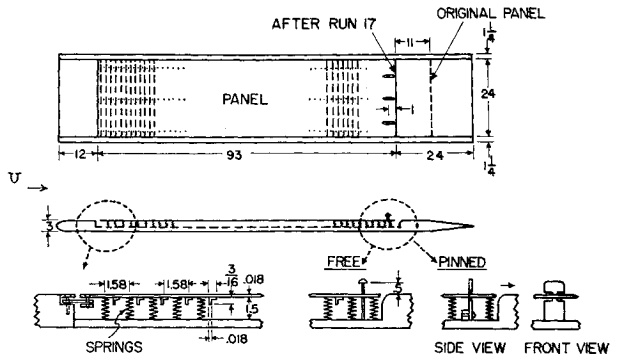

Fig. 1 Panel test model and wooden frame

mensional behavior of the panel.‖ The springs in each of the three rows were spaced 1.58 in. apart in the stream direction. Since the wavelengths anticipated were of the order of 24 in., it was felt that the discrete springs adequately represented a continuous elastic foundation.

The trailing edge, when kept free, was limited to about $\frac{1}{2}$-in. vertical motion above the undeformed position by three loosely fitting bolts. These were placed in only after run 17, when excessive motion damaged the trailing edge. When the trailing edge was pinned instead of free, the three bolts were replaced by three plastic knife edges. Slotted holes were made in the panel to prevent axial tension forces from developing when the panel deflected vertically. The bottom of the wooden box frame was covered by a wooden panel with numerous 1-in.-diam holes to allow tunnel static pressure to be developed on the inside of the aluminum test panel.

A square grid of black lines was painted on the panel for ease in observing the panel behavior. The distance between lines was roughly 6 in., and the lines perpendicular to the flow were numbered from 0 to 16, starting at the leading edge. Eight SR-4 strain gages, spaced 3.2 in. apart in the stream direction, also were placed on the underside of the panel near its midsection. These were used to obtain frequency and phasing behavior.

b. Static and Vibration Tests

Each helical coil spring had a length of $1\frac{1}{2}$ in., a diameter of $\frac{1}{2}$ in., and could be compressed to bottom without buckling. A typical spring was tested and found to be fairly linear over a wide range, with a spring rate of 0.88 lb/in.

The panel was vibrated in its wooden supporting frame by attaching an electrodynamic shaker to the panel centerline about 8 in. from the leading edge. Salt was sprinkled over the panel to determine the position of the node lines. The experimental modes and frequencies, together with theoretical ones computed from the spring and mass properties (see Sec. 3a), are given in Fig. 2 for the higher modes ($n = 7$ to $n = 11$). The observed frequencies are in reasonable agreement with those calculated. Although the observed node lines are not as clear cut or uniformly spaced as the theoretical ones, they do resemble the calculated ones, and the trends with n are good. As can be expected from the theoretical analysis, the lower modes ($n = 1, 2, 3$, etc.) are too close together to be excited separately and observed by this single shaker.

The panel also was vibrated with the shaker located 16.5 in. from the trailing edge. These mode shapes and frequencies were quite similar to those obtained with the shaker in the forward position.

c. Mounting in Tunnel

The test panel and its supporting wooden box frame were mounted in the Massachusetts Institute of Technology Wright

‖ An oil-can effect existed originally in the forward part of the sheet. This necessitated somewhat larger-size stiffeners in this vicinity to get rid of this three-dimensional effect.

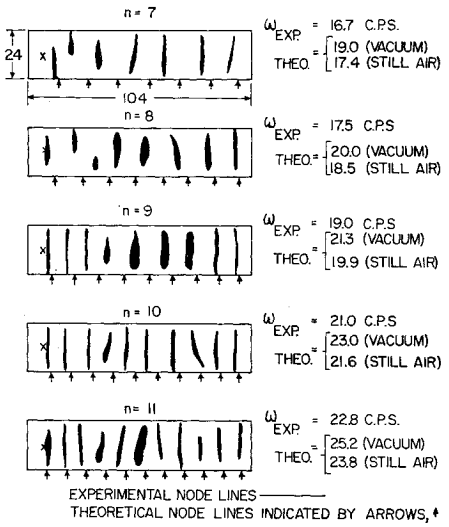

Fig. 2 Vibration modes of panel

Brothers low-speed wind tunnel. The tunnel has a $7\frac{1}{2}$- × 10-ft elliptical test section that is vented to approximately atmospheric pressure and is capable of speeds of 140 mph at atmospheric pressure. The wooden box frame on which the test panel lay was placed between two endplates, as shown in Fig. 3. These $\frac{1}{2}$-in. plywood endplates were used to try to assure two-dimensionality of the flow. The center portion of one of them was replaced by Plexiglas to allow visual observation of the test panel surface. The wooden box frame could be changed in angle of attack somewhat in order to adjust the pressure and velocity distribution over the panel. Three Pitot-static tubes were placed about 12 in. over the centerline of the panel to measure the velocity. Later on in the test program, nine more Pitot-static tubes were added to survey the pressure and velocity distribution over the panel more accurately.

The static vertical deflection of the panel under the action of the air forces could be estimated visually by reading it against a grid of six long black lines $\frac{1}{4}$ in. apart ruled on the inside face of one of the wood beams of the supporting box frame. The panel surface itself with its 6-in.^{2} grid could be viewed through the Plexiglas endplate and the wind tunnel window. Movies could be taken from this position.

d. Flutter Test Procedure

During a typical flutter test run, the tunnel speed was raised to a given value and held. For this speed, the tunnel Pitot-static tube and the three panel Pitot-static tubes were read, thereby giving the reference tunnel setting and the actual velocity at the panel. The static deflection shape of the panel then was recorded by visual observation. The foregoing test runs were repeated in small tunnel velocity increments until significant vibrational activity or flutter was observed visually over the panel surface. Then, both oscillograph records of the strain gages and 16-mm movies of the panel surface were taken.

The test program carried out included 126 runs and was a consequence of attempts to repeat results, to investigate both free and pinned trailing-edge conditions, to minimize effects of nonuniform pressure and velocity distributions over the panel, and to determine detailed pressure and velocity distributions over the panel.

e. Test Results

The static deflections of the panel for different angle-of-attack settings and tunnel settings are shown in Fig. 4. A prominent static depression near the leading edge clearly is visible. This was attributed to undesirable nonuniform pres-

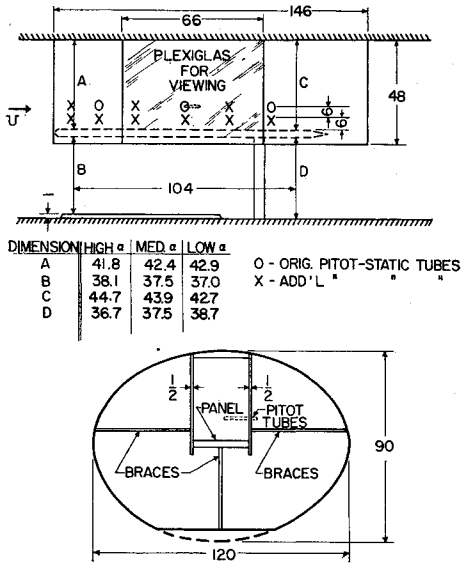

Fig. 3 Mounting in tunnel

sure and velocity distributions over the panel[2] and was remedied somewhat by increasing the angle of attack between the endplates. Later on in the test program, more accurate pressure and velocity surveys were made, revealing velocity variations of the order of 6% over the length of the panel for the high angle-of-attack case. Also clearly visible in Fig. 4 is a sinusoidal pattern of about a 2-ft wavelength that developed near the trailing edge on many of the runs, particularly on runs 114 through 121, the low angle-of-attack, pinned case.

Flutter was observed for many of the runs. Except for run 17, when the panel trailing edge fluttered violently and was damaged, the flutter tended to be nondestructive and limited in amplitude, so that it could be viewed for relatively long periods of time. The double amplitude reached values of over $\frac{1}{2}$ in. on many of these runs. Considerable variation in the flutter speeds of the order of 15% was evident, particularly between the different angle-of-attack settings.[2] There was a lesser change between the free and pinned end conditions. It was felt that the results for the high angle-of-attack case were the most reliable, since these had the smallest static depression at the leading edge and the smallest pressure and velocity variation over the panel surface. The large static

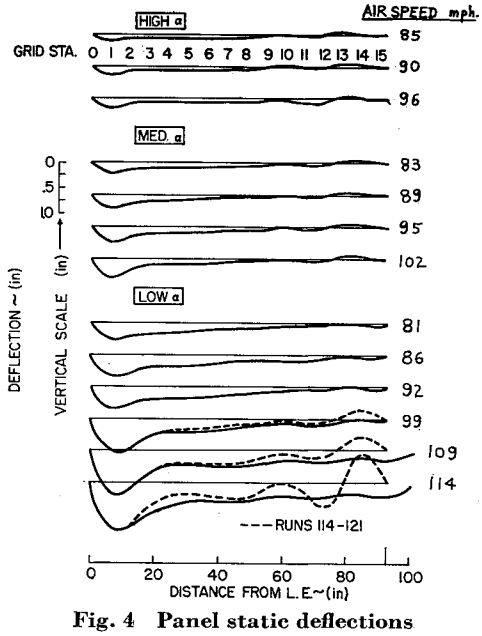

Fig. 4 Panel static deflections

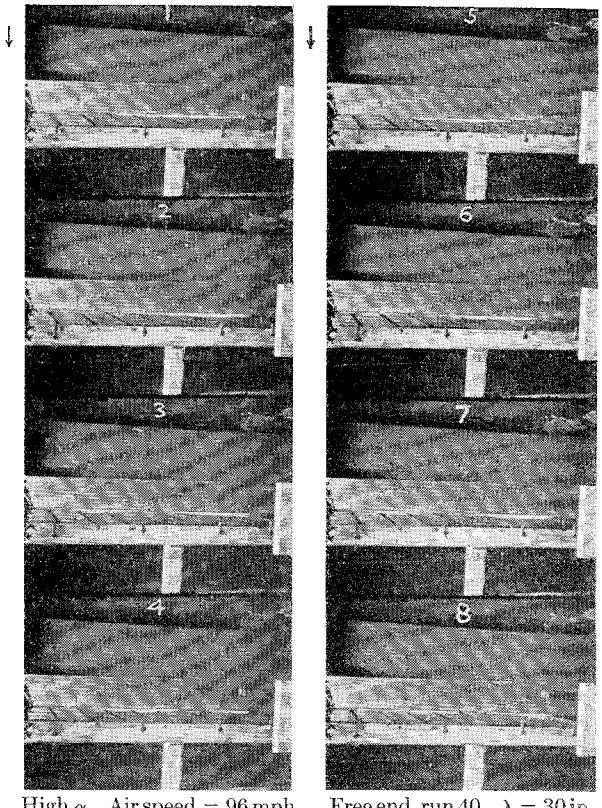

High α. Air speed = 96 mph Free end, run 40. $\lambda = 30$ in.
Film 3
$c + U \approx 35$ fps

Fig. 5 Typical movie record

depression, in addition to aerodynamic effects, shortened the effective length of the panel and may have introduced midplane tension and structural nonlinear effects into the panel behavior.

Movies of many of the flutter test runs were taken with a 16-mm camera at 64 frames/sec. The more interesting shots were compiled together into a single 400-ft film strip representing 22 different runs. The movie films recorded both steady flutter and the onset of flutter in some cases. A typical flutter film sequence is shown in Fig. 5 for the high angle-of-attack case. Analysis of this and other flutter film sequences[2] in the film strip indicated a flutter frequency of about 14 cps, a wavelength of about 2 to $2\frac{1}{2}$ ft, and a wave speed of about 35 fps. The waves generally appeared to be traveling downstream, although there seemed to be some small "sticking" or standing wave component present in some of them. Some small distortion of the traveling waves from a pure sinusoidal shape was evident, particularly for the larger amplitudes of wave motion.

Oscillograph records of many of the flutter test runs were taken. A typical oscillograph record for the same run as the film strip is given in Fig. 6. The eight strain-gage traces are shown, giving the frequency and phasing of the different locations. Since the gages were all roughly similar in sensitivity, a measure of the amplitudes also is obtained for these locations. Analysis of this and other oscillograph records indicated evidences of standing waves with some small traveling-wave components present. The frequencies average about 14 cps. Some other oscillograph records, taken slightly below the visually observed flutter, showed strong evidences of traveling waves.

Summarizing, it appeared that definite flutter of a generally traveling wave-type character was obtained for this panel, with the approximate characteristics given in Table 1. The waves generally appeared to be traveling downstream, although there seemed to be some "sticking" or standing wave components present near the center of the panel. The flutter

speed was not affected much by the trailing-edge condition, i.e., whether pinned or free there. Prior to flutter, the panel assumed a sinusoidal static deflection shape of about 2-ft wavelength in the vicinity of the trailing edge. (In one case, run 121, this became a rather sizable deflection.) There appeared also a prominent static depression in the vicinity of the leading edge which was remedied somewhat by altering the angle of attack and hence pressure distribution over the panel.

In any future experimental work along these lines, care should be taken 1) to insure two-dimensional panel behavior by providing sufficiently large angle stiffeners, and 2) to maintain uniform pressure and velocity distributions over the panel by proper wall contouring and venting.

3. Theory

a. Free Vibration Modes

The equation for the deflection $w(x,t)$ of a two-dimensional panel resting on a continuous elastic foundation is

$$D(\partial^4 w/\partial x^4) + Kw = \Delta p - m(\partial^2 w/\partial t^2) \tag{1}$$

where, for the present panel,

$$\begin{aligned} D &= 5.61 \text{ lb-in.} \\ K &= 0.0696 \text{ lb/in.}^3 \\ m &= 5.79 \times 10^{-6} \text{ lb-sec}^2/\text{in.}^3 \\ l &= 104 \text{ in.} \\ \rho_\infty &= 0.1148 \times 10^{-6} \text{ lb-sec}^2/\text{in.}^4 \end{aligned} \tag{2}$$

For free vibrations in a vacuum, $\Delta p = 0$. Using the standard separation of variables technique and putting in the appropriate boundary conditions (pinned at $x = 0$, free at $x = l$), one obtains the natural vibration frequencies:

$$\omega_n = [(K/m) + (n + \tfrac{1}{4})^4(\pi^4 D/ml^4)]^{1/2} \tag{3}$$

The corresponding natural mode shapes ϕ_n are

$$\phi_n = \sin\left(n + \frac{1}{4}\right)\frac{\pi x}{l} + \frac{(-1)^n}{2^{1/2}\sinh(n+\frac{1}{4})\pi} \times \sinh\left(n + \frac{1}{4}\right)\frac{\pi x}{l} \tag{4}$$

For the higher values of n, these modes resemble pure sine waves except in the immediate vicinity of the trailing edge. The nth mode has n node lines spaced approximately a distance $l/(n + \frac{1}{4})$ apart, starting from the leading edge.

For the present panel, the theoretical frequencies and node lines for free vibrations in a vacuum for values of $n = 7$ to $n = 11$ are shown in Fig. 2. The fundamental frequency for $n = 1$ is calculated at 17.5 cps. It is seen that the lower modes are spaced very closely together in frequency.

For actual vibrations in still air, an additional virtual mass of air should be included with the panel mass. This is shown in Sec. 3d to result in a total mass # of approximately

$$m[1 + (2\rho_\infty l/m\pi n)] = m[1 + (1.312/n)] \tag{5}$$

These still air frequencies also are shown in Fig. 2. The mode shapes are unchanged by this additional air mass.

b. Infinite Panel: No Internal Damping

The flutter of an infinite panel in two-dimensional incompressible flow has been investigated by Miles.[1] There he used an axis system fixed to the air at rest and considered the infinite panel to be moving with velocity U in the negative x direction. The equation of motion for such an undamped

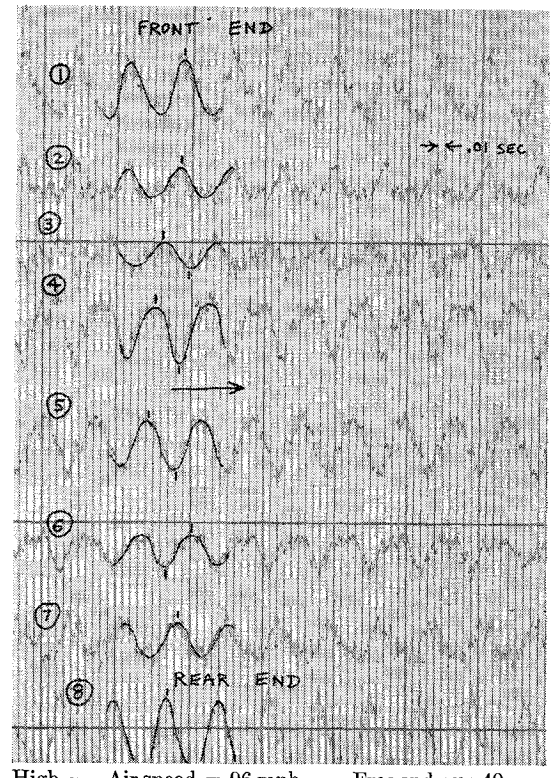

High α. Air speed = 96 mph Free end, run 40.
Film 3 $\omega \approx 14.3$ cps

Fig. 6 Typical oscillograph record

panel on an elastic foundation is

$$D(\partial^4 w/\partial x^4) + Kw + m[(\partial/\partial t) - U(\partial/\partial x)]^2 w = \Delta p \tag{6}$$

Miles has shown that for traveling wave solutions of the form

$$w(x,t) = w_0 e^{i(ct-x)2\pi/\lambda} \tag{7}$$

the aerodynamic distribution** is

$$\Delta p = \rho_\infty(2\pi/\lambda)c^2 w_0 e^{i(ct-x)2\pi/\lambda} \tag{8}$$

Substituting Eqs. (7) and (8) into (6), one obtains

$$(\zeta + 1)^2 - \zeta_0^2 + \mu\zeta^2 = 0 \tag{9}$$

where

$$\mu = \rho_\infty \lambda/2\pi m \tag{10}$$

$$c_0 = \left[\frac{K}{m}\left(\frac{\lambda}{2\pi}\right)^2 + \frac{D}{m}\left(\frac{2\pi}{\lambda}\right)^2\right]^{1/2} \tag{11}$$

where c_0 is the wave speed in the absence of air ($\rho_\infty = 0$), and μ is the mass density ratio of the panel (for air flow on top side of panel only). Solving Eq. (9) for ζ, Miles obtained the following expression for the wave speed relative to the panel:

$$c + U = [1/(1 + \mu)]\{\mu U \pm [(1 + \mu)c_0^2 - \mu U^2]^{1/2}\} \tag{12}$$

Complex values of c possessing negative imaginary parts represent instabilities. These occur for

$$U/c_0 > [(1 + \mu)/\mu]^{1/2} \tag{13}$$

This criterion is plotted in Fig. 7. The corresponding wave speed relative to the panel is

$$c + U = [\mu/(1 + \mu)]U \tag{14}$$

In the foregoing criterion, both μ and c_0 are functions of the

For still air on both sides of panel, and also for high n, where $\sin n\pi x/l$ is a reasonable approximation to the mode shape.

** The pressure acting on the bottom side is assumed constant at p_∞. The presence of air at the bottom side is examined in the Appendix and found to be small for the low μ of interest here.

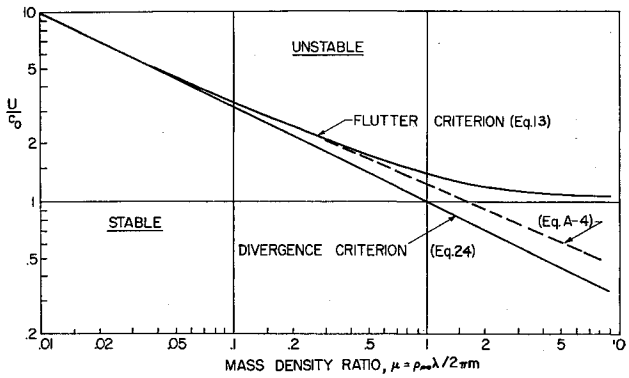

Fig. 7 Flutter and divergence criteria (infinite panel)

wavelength; hence the flutter speed will vary with the wavelength. For this panel on an elastic foundation, the variation of flutter speed U_F with λ is shown in Fig. 8. Unlike the case of a membrane or a plate where the minimum flutter speed occurs for $\lambda \to \infty$, the panel on an elastic foundation possesses a minimum flutter speed at a finite value of λ. This wavelength for minimum flutter speed is

$$\lambda_{\min} = 2\pi(D/K)^{1/4} f_1 \tag{15}$$

where f_1 is a correction factor given by

$$f_1 = [(1.5 + \mu)/(0.5 + \mu)]^{1/4} \tag{16}$$

and varies from $f_1 = 1$ at high values of μ to $f_1 = 1.316$ as $\mu \to 0$.

For the present panel, the characteristics at flutter as calculated numerically are given in Table 1. Below the flutter speed, a multitude of undamped traveling wave solutions are possible corresponding to different wavelengths λ. The wave speeds relative to the panel $c + U$ are plotted in Fig. 9 for different wavelengths and airspeeds.

It is informative to investigate the unstable behavior of the panel above the flutter speed and to determine how fast the instability sets in. In terms of a coordinate system X fixed to the moving panel, the traveling wave solutions of Eq. (7) can be written as

$$w(X,t) = w_0 e^{\,i[(c_R+U)t - X](2\pi/\lambda)} e^{-c_I t} \tag{17}$$

where c_R and c_I are the real and imaginary parts of c. As a measure of the instability, the amplification A is introduced and is defined as the ratio of the wave amplitudes during the time it takes the wave to travel one wavelength. From Eq. (17), it follows that

$$A = e^{-2\pi c_I/(c_R+U)} \tag{18}$$

For this panel, the amplification A is shown (the $DR = 0$ case) in Fig. 10 for the most critical wavelength $\lambda = 25$.

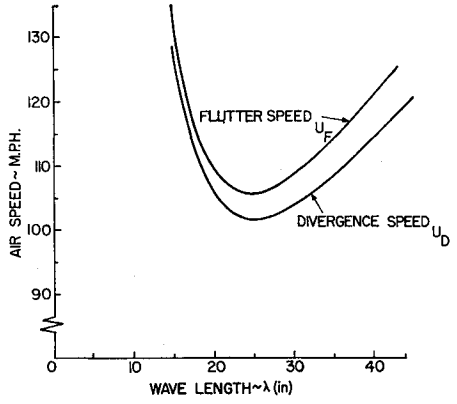

Fig. 8 Flutter and divergence speed vs λ (infinite panel)

The instability sets in very sharply after U_F is exceeded, and the amplification A reaches values of the order of 100 for 2 or 3 mph above the flutter speed. During this time, the wave speed $c_R + U$ remains about constant at 11.4 fps.

c. Infinite Panel: Internal Damping Present

Consider next the effect of adding internal damping to the structure. The basic equation of motion is then

$$D\frac{\partial^4 w}{\partial x^4} + Kw + m\left(\frac{\partial}{\partial t} - U\frac{\partial}{\partial x}\right)^2 w + B\left(\frac{\partial}{\partial t} - U\frac{\partial}{\partial x}\right) w = \Delta p \tag{19}$$

and the corresponding equation in ζ would read

$$(\zeta + 1)^2 + \zeta_0^2 + \mu\zeta^2 - i(B\lambda/2\pi mU)(\zeta + 1) = 0 \tag{20}$$

Solving the Eq. (20) for ζ now gives

$$c + U = \frac{U}{1+\mu}\left\{\mu + \frac{iG}{2} \pm \left[\left\{\zeta_0^2(1+\mu) - \mu - \frac{G^2}{4}\right\} + i\mu G\right]^{1/2}\right\} \tag{21}$$

where $G \equiv B\lambda/2\pi mU$ is a measure of the additional damping present in the structure. Unstable solutions now will occur if the imaginary part of the radical has an absolute value greater than $G/2$, that is, if

$$\frac{G}{2} < \frac{1}{2^{1/2}}\left\{+\left[\left\{\zeta_0^2(1+\mu) - \mu - \frac{G^2}{4}\right\}^2 + \mu^2 G^2\right]^{1/2} - \zeta_0^2(1+\mu) + \mu + \frac{G^2}{4}\right\}^{1/2} \tag{22}$$

By routine algebra, the inequality (22) reduces simply to

$$\zeta_0^2 < \mu \tag{23}$$

It is interesting to note that this criterion does not depend on the magnitude of the damping G present in the structure. Hence, for any small amount of damping present, instability will set in for

$$U/c_0 > (1/\mu)^{1/2} \tag{24}$$

rather than the somewhat higher value given previously by Eq. (13) for the completely undamped case. This new criterion is shown in Fig. 7 together with the previous criterion for the undamped panel. At the onset of this new instability, the corresponding real part of the radical appearing in Eq. (21) equals $-\mu$, and the wave speed relative to the panel $c + U$ becomes equal to zero. This indicates a static divergence-type instability rather than the traveling wave flutter-type instability obtained previously for the undamped case.

The presence, then, of a very small amount of damping appears sufficient to lower the instability speed of the panel and to change its character from a traveling wave flutter-type instability to a static divergence-type instability. This behavior has been noted also by others, for example, Leonard and Hedgepeth,[4] for thin circular cylinders in an airstream, and Landahl,[5] in a study of the boundary layer on a flexible panel.

In the criterion of Eq. (24), the instability speed again varies with wavelength λ. This divergence speed is shown plotted vs λ in Fig. 8. The wavelength for minimum divergence speed is given by Eq. (15) with $f_1 = 1.316$.

For the present panel with a small amount of damping present, the characteristics at instability (divergence now) as calculated numerically are given in Table 1. Below the

divergence speed, the traveling wave solutions corresponding to different wavelengths are all damped traveling waves.

It is again informative to investigate the unstable behavior of the panel above the divergence speed. The internal damping present in the panel foundation can be expressed as $B = 2(DR)[Km]^{1/2}$, where (DR) represents the familiar critical damping ratio and is of the order of 0.01 for this metallic structure. Using this, the damping parameter G becomes

$$G = [(DR)/\pi](K/m)^{1/2}(\lambda/U) \tag{25}$$

For the present panel, the complex wave speed $c + U$ was computed for airspeeds above divergence and for several values of damping ratio DR. The corresponding amplification A is given in Fig. 10. Only the behavior of the minimum wavelength $\lambda = 25$ in. is shown, since the other λ's show similar, less critical trends.

From Fig. 10, the transition between the undamped and the damped panel becomes clear. For low damping ratios, the divergence-type instability represented by Eq. (24) is a very mild one, and the amplification A does not become significant until the airspeed approaches that for the flutter-type instability represented by Eq. (13). In a corresponding manner, the wave speed $c_R + U$ changes from zero to the value for the flutter-type instability given by Eq. (14). For large damping ratios, the divergence-type instability does become significant and is associated with very low-speed traveling waves. The interesting destabilizing effect of internal damping in the airspeed region between 101.5 and 105.5 mph is to be noted.

Table 1 Summary of experimental and theoretical results

	Experiment	Theory (infinite)	Theory (finite)
Flutter speed, mph	95	105.5	103.1
Wavelength, in.	27	25	24.5
Wave speed, fps	35	11.4	6.9
Frequency, cps	14	5.5	3.4
μ	0.079	0.079	...
$\bar{\mu}$	0.656	...	0.656
Divergence speed, mph	...	101.5	101.5
Wavelength, in.	...	25	26

Some simple expressions are given below for the flutter and divergence speeds of these infinite panels on elastic foundations. Simple algebraic manipulation of the appropriate equations gives the dynamic pressure at flutter and at divergence, as

$$\frac{1}{2}\rho_\infty U_F^2 = \frac{1+\mu}{2}\left[\left(\frac{1.5+\mu}{0.5+\mu}\right)^{1/4} + \left(\frac{0.5+\mu}{1.5+\mu}\right)^{3/4}\right] K^{3/4}D^{1/4} \tag{26}$$

$$\tfrac{1}{2}\rho_\infty U_D^2 = 0.878K^{3/4}D^{1/4} \tag{27}$$

The appropriate value of μ is found through consideration of Eqs. (10, 15, and 16).

d. Finite Panel

For a finite length panel, the differential equation to be solved is given by Eq. (1) subject to the appropriate boundary conditions. For simplicity, the panel is assumed to be pinned at both ends.†† The aerodynamic pressure for air acting on the top side only can be expressed as[6]

$$\Delta p = \frac{\rho_\infty}{\pi}\int_0^l \left(\frac{\partial^2 w}{\partial t^2} + U\frac{\partial^2 w}{\partial t \partial x}\right)\ln\left|\frac{x-\xi}{l}\right| d\xi + \frac{\rho_\infty}{\pi}\int_0^l \left(U\frac{\partial w}{\partial t} + U^2\frac{\partial w}{\partial x}\right)\frac{1}{x-\xi}\,d\xi \tag{28}$$

As the general solution of the integro-differential equation given by Eqs. (1) and (28) is extremely difficult, a Galerkin type solution will be used, assuming

$$w(x,t) = \sum_{n=1}^{N} q_n(t)\sin\frac{n\pi x}{l} \tag{29}$$

These modes satisfy the pinned-end boundary conditions. Furthermore, the aerodynamic pressure will be assumed to be that for an infinitely long wavy wall of the shape given by Eq. (29). This is reasonable except in the immediate vicinity of the leading and trailing edges, particularly for the high modes (large n) of interest here. Using Eq. (29) the aerodynamic pressure Δp Eq. (28) reduces to (see also Flax[7])

$$\Delta p = \sum_{n=1}^{N}\left\{\left[-\frac{\rho_\infty l}{n\pi}\frac{d^2 g_n}{dt^2} + \rho_\infty U^2\frac{n\pi}{l}q_n\right]\sin\frac{n\pi x}{l} - \left[2\rho_\infty U\frac{dq_n}{dt}\right]\cos\frac{n\pi x}{l}\right\} \tag{30}$$

Placing this expression together with Eq. (29) into the basic panel equation (1), applying Galerkin's method, and non-

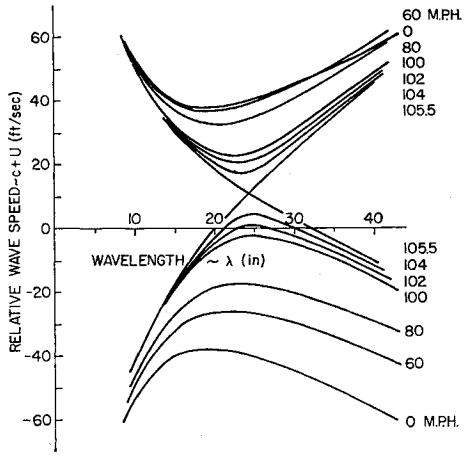

Fig. 9 Wave speed $c + U$ for undamped panel (infinite panel)

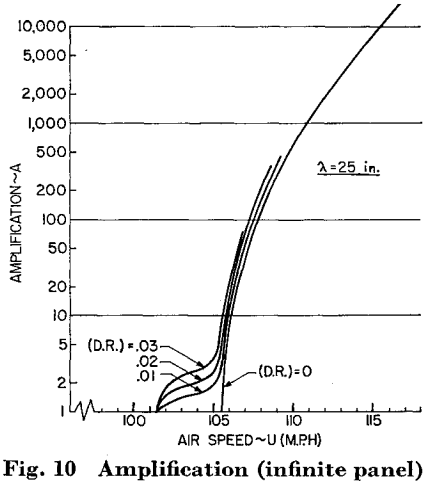

Fig. 10 Amplification (infinite panel)

†† The higher modes are of interest here, and for these, the different boundary conditions do not affect the modes and frequencies much except in the immediate vicinity of the trailing edge.

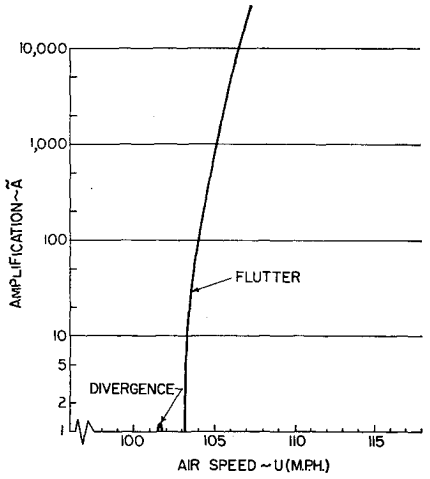

Fig. 11 Amplification (finite panel)

dimensionalizing results in the series of ordinary differential equations:

$$\left[1 + \frac{\tilde{\mu}}{n}\right]\frac{d^2q_n}{d\bar{t}^2} + [n^4\pi^4 + \bar{K} - Qn\pi]q_n + \left[\frac{Q\tilde{\mu}}{\pi}\right]^{1/2} \sum_{n+r=\text{odd}}^{n,r=1,2,\ldots N} \left(\frac{8n}{n^2 - r^2}\right)\frac{dq_r}{d\bar{t}} = 0 \quad (31)$$

where the foregoing summation is taken over the r terms for which $n + r$ is an odd integer, and the nondimensional parameters $\bar{t}$, $\tilde{\mu}$, Q, and $\bar{K}$ have been introduced.

Consider now the coupling between the n and $n + 1$ modes. Upon seeking solutions of the form $\exp(\bar{s}\bar{t})$, Eqs. (31) become

$$\left\{\bar{s}^2\left[1 + \frac{\tilde{\mu}}{n}\right] + [n^4\pi^4 + \bar{K} - n\pi Q]\right\} q_n + \left\{\bar{s}\left[\frac{Q\tilde{\mu}}{\pi}\right]^{1/2}\frac{8n}{n^2 - (n+1)^2}\right\} q_{n+1} = 0 \quad (32)$$

$$\left\{\bar{s}\left[\frac{Q\tilde{\mu}}{\pi}\right]^{1/2}\frac{8(n+1)}{(n+1)^2 - n^2}\right\} q_n + \left\{\bar{s}^2\left[1 + \frac{\tilde{\mu}}{n+1}\right] + [(n+1)^4\pi^4 + \bar{K} - (n+1)\pi Q]\right\} q_{n+1} = 0$$

Setting the determinant of the preceding equations equal to zero yields the characteristic equation in $\bar{s}$:

$$A_4\bar{s}^4 + A_2\bar{s}^2 + A_0 = 0 \quad (33)$$

where

$$A_4 = \left(1 + \frac{\tilde{\mu}}{n}\right)\left(1 + \frac{\tilde{\mu}}{n+1}\right)$$

$$A_2 = \left(1 + \frac{\tilde{\mu}}{n}\right)[(n+1)^4\pi^4 + \bar{K} - (n+1)\pi Q] + \left(1 + \frac{\tilde{\mu}}{n+1}\right)[n^4\pi^4 + \bar{K} - n\pi Q] + \frac{64}{\pi}\frac{n(n+1)}{(2n+1)^2}\tilde{\mu}Q \quad (34)$$

$$A_0 = [n^4\pi^4 + \bar{K} - n\pi Q][(n+1)^4\pi^4 + \bar{K} - (n+1)\pi Q]$$

The roots $\bar{s}$ of the characteristic equation, Eq. (33), are examined as Q increases from zero. Real positive roots represent divergence instabilities, whereas complex roots with positive real parts represent flutter instabilities.

First, the static divergence behavior is examined. This occurs when $A_0 = 0$, which implies

$$Q = (n^4\pi^4 + \bar{K})/n\pi \quad (35)$$

For the present panel, $\bar{K} = 1.46 \times 10^6$. The minimum Q occurs for $n = 8$, and the corresponding values at divergence are $Q = 73{,}570$, $U = 101.5$ mph, and $\lambda = 2l/n = 26$ in. These values are shown in Table 1 and agree well with those obtained for the infinite panel.

Next, the complete dynamic behavior is examined. Equation (33) can be solved to give the four roots $\bar{s}$ as

$$\bar{s} = \pm\left\{\frac{-A_2 \pm [A_2^2 - 4A_4A_0]^{1/2}}{2A_4}\right\}^{1/2} \quad (36)$$

Flutter (dynamic instability) will occur only if the inner radical becomes imaginary, i.e., if $A_2^2 - 4A_4A_0 < 0$. Placing the values of Eq. (34) into this criterion, it can be shown that flutter can occur only for negative values of $[n^4\pi^4 + \bar{K} - n\pi Q]$, that is, only after the divergence speed has been exceeded. This result also has been shown more generally for an infinite number of modes by Flax.[7] For the present panel, the four roots $\bar{s}$ associated with coupling between the eighth and ninth modes were computed for various values of Q. At low speeds, these roots represent two undamped steady sinusoidal oscillations. Then static divergence sets in for a very narrow band of speeds from 101.55 to 101.77 mph. Above this band, two undamped steady sinusoidal oscillations are present again. Finally, at speeds above 103.13 mph, flutter instability occurs. The characteristics at flutter as calculated from this analysis are shown in Table 1. These agree well with the infinite panel values of flutter speed and wavelength but are lower somewhat in frequency and wave speed.

The rate of growth associated with these instabilities is of interest. For this finite panel, the amplification $\tilde{A}$ is introduced and is defined as the ratio of amplitudes during a time interval of 0.295 sec. This is the time for one oscillation at the flutter frequency and is chosen to make the $\tilde{A}$ of the finite panel somewhat comparable to the A of the infinite panel. Then

$$\tilde{A} = e^{0.295(s)_{\text{real}}} \quad (37)$$

$\tilde{A}$ is shown plotted vs airspeed in Fig. 11. Again, the divergence instability is very mild compared to the strong instability associated with flutter. This, together with the narrow speed band associated with divergence, seems to indicate that flutter will be the principal instability, at least for this simplified two-mode example.

The undamped steady oscillations occurring below and above the divergence speed band were investigated in more detail. Figure 12 shows the variation of frequency ω with airspeed. The corresponding deflection shapes associated with

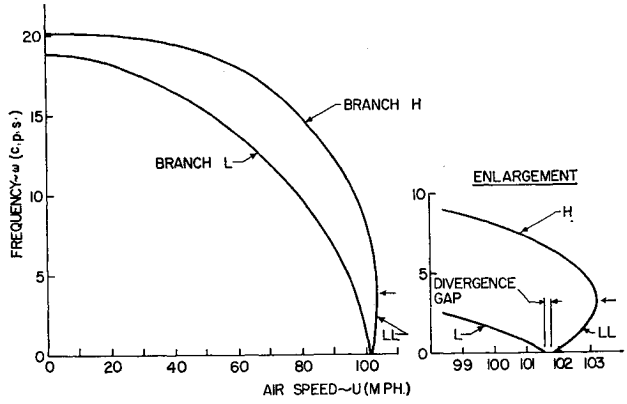

Fig. 12 Frequency of steady oscillations (finite panel)

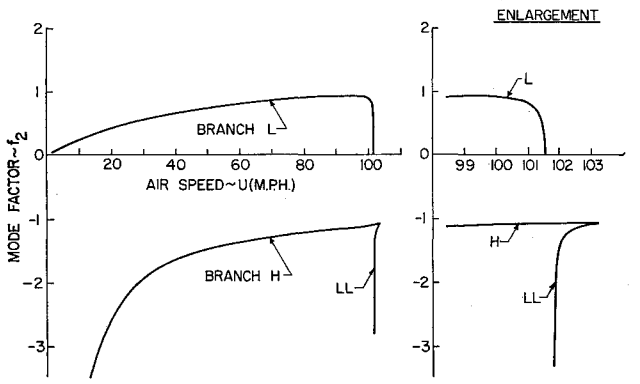

Fig. 13 Mode factor f_2 (finite panel)

these steady oscillation frequencies ω are

$$w(x,t) = \cos\omega t \sin(n\pi x/l) + f_2 \sin\omega t \sin(n+1)(\pi x/l) \tag{38}$$

where

$$f = \frac{(2n+1)}{8n}\left[\frac{\pi}{Q\tilde{\mu}}\right]^{1/2}\left\{\frac{(n^4\pi^4 + \bar{K} - n\pi Q)}{|\bar{s}|} - |\bar{s}|\left(1 + \frac{\tilde{\mu}}{n}\right)\right\} \tag{39}$$

The mode coupling factor f_2 plays an interesting role in Eq. (38). Values of this factor $f_2 = 0$ and $f_2 \to \infty$ represent pure standing waves in the $\sin n\pi x/l$ and $\sin(n+1)\pi x/l$ modes, respectively, whereas values of $f_2 = +1$ and $f_2 = -1$ represent approximately traveling waves in the upstream and downstream directions, respectively. This latter fact can be seen by rewriting the deflection shape, Eq. (38), equivalently as

$$\begin{aligned} w(x,t) &\approx \sin[\omega t + (n+\tfrac{1}{2})(\pi x/l) - 45°] \quad \text{for } f_2 = +1 \\ &\approx \sin[\omega t - (n+\tfrac{1}{2})(\pi x/l) + 45°] \quad \text{for } f_2 = -1 \end{aligned} \tag{40}$$

In obtaining the foregoing, it has been assumed that, near the center portion of a long panel, $\cos \pi x/2l \approx \sin \pi x/2l \approx 1/2^{1/2}$. This approximation is particularly good when n is large. The variation of the factor f_2 with airspeed for the present panel is shown in Fig. 13. The behavior of these steady oscillations then becomes clear. At very low speeds, they represent almost pure standing waves. As speed increases, they develop rapidly into two traveling waves, the lower frequency branch L moving upstream and the higher one H moving downstream. At the divergence speed, divergence occurs in the lower mode 8. Later, divergence occurs in the higher mode 9. Above the narrow divergence gap, the lower frequency branch LL reappears and rapidly becomes a traveling wave now moving downstream. At the flutter speed, the two traveling waves coalesce and give rise to unstable oscillations. A sketch of the oscillations at flutter is given in Fig. 14. The dashed lines indicate the eighth and ninth mode components making up the total deflection. The traveling wave character of these oscillations is clearly apparent.

The general behavior of the two-degree-of-freedom finite panel analysis closely resembles the infinite panel analysis. The divergence speed, the mild character of divergence, the undamped traveling waves moving in opposite directions below divergence and in the same direction above divergence (compare with Fig. 9), and finally their merging together to form a strong flutter all are present here. The characteristics at divergence and flutter also are quite similar. Presumably, the presence of more modes and some additional internal damping would bring the results of the finite and infinite panel analyses more closely in line with one another, particularly for instabilities occurring at high values of n. Thus, a smooth transition between the finite panel standing wave analysis at low values of n to the infinite panel traveling wave analysis at high values of n is observed.

Some simple expressions are given below for the divergence of these finite panels on elastic foundations. Using Eq. (35), the onset of divergence can be defined by the nondimensional parameter Q. For the values of $\bar{K} > 1500$, the divergence can be approximated by

$$Q \approx 1.756\,\bar{K}^{3/4} \tag{41}$$

$$n \approx 0.242\bar{K}^{1/4} \text{ (nearest integer)} \tag{42}$$

For $\bar{K} < 1500$, the divergence is given by Eq. (35) with $n = 1$. As discussed previously, this divergence criterion represents a lower bound on the occurrence of instability.

4. Comparison of Experiment and Theory

The experimental test results indicated generally a traveling wave-type flutter with the approximate characteristics given in Table 1. The theoretical results, showing essentially similar behavior from both the infinite panel and finite panel point of view, indicated a strong traveling wave-type flutter developing with the characteristics given in Table 1. In addition, a much milder instability of static-divergence-type also was shown to exist at a slightly lower speed and with essentially the same wavelength.

Comparing these experimental and theoretical results, it is seen that there is good agreement in the flutter speed and wavelength but rather poor agreement in the wave speed and frequency at flutter. Below the flutter speed, the observed small static deflections agree well in wavelength with those of theory.

The poor agreement found here in wave speed and frequency at flutter is typical of other aeroelastic phenomena in which the flutter frequency is less accurately predicted than the flutter speed. Looking at Fig. 9 or at Fig. 12, it is seen that small changes in air speed have great effects on the wave speed and frequency in the vicinity of the flutter speed. The prediction of $c + U$ and ω here seems generally more difficult than that of air speed.

Some specific factors that may have contributed to the poor agreement in wave speed and frequency are given below:

1) *Static depression at leading edge.* This shortened the effective length of the panel and may have introduced midplane tension and structural nonlinearities into the panel behavior. It is felt that this effect was the primary reason for the scatter in the experimental results at high, medium, and low angles of attack. Also, this probably contributed to the appearance of the large static deflections of runs 114 through 121.

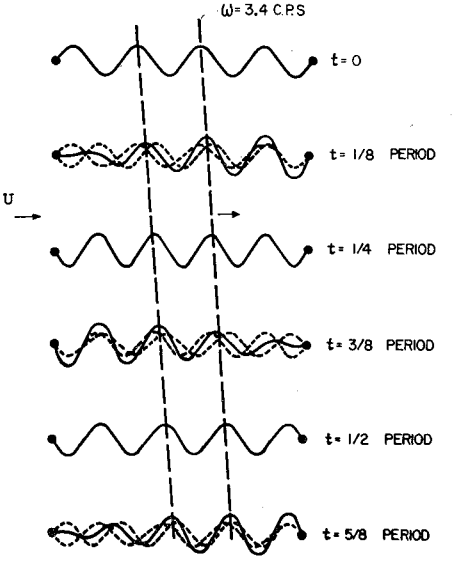

Fig. 14 Oscillations at flutter (finite panel)

2) *Cavity effect of still air on bottom side of panel.* The effect of still air of infinite depth on the bottom side of the panel was investigated in the Appendix and found to be negligible for this panel. However, perhaps for the finite depth of about $2\frac{1}{2}$ in. here, the cavity resonance effect may be more appreciable. Also, the large amplitudes of the flutter deflections may have had an influence here.

3) *Buffeting at trailing edge.* There may have been some forcing oscillations caused by rough flow at the trailing edge, particularly when the edge was free. The somewhat similar experimental results obtained for the case of free and pinned edges seem to minimize this source of disturbance.

4) *Boundary layer effects.* The effects of a boundary layer in influencing panel flutter behavior recently have been suggested. Some investigations have been carried out by Miles,[8] and, more recently, Landahl[5] studied the stability of a boundary layer in the presence of a flexible wall. It is believed that this specific panel lies outside the range of any such significant effects.

5. Conclusions

Experimentally, definite flutter was observed for a specific panel in this subsonic flow. The flutter was of a traveling-wave type, although there seemed to be some standing-wave component present near the center of the panel. Below the occurrence of flutter, the panel assumed a small static sinusoidal deflection shape over the rear half of the panel.

Theoretically, it has been shown that a finite panel analysis gives essentially the same behavior as the infinite panel analysis for high values of n (or l/λ). Thus, a smooth transition is demonstrated between the finite panel, standing-wave analysis at low values of n to the infinite panel, traveling-wave analysis at high values of n. Also, it has been shown that, although a mild static-divergence-type instability exists for these panels, the principal instability will be a traveling-wave, flutter-type instability. The addition of internal damping to these panels was shown to have an interesting destabilizing effect in the region between the divergence speed and the flutter speed.

Comparison of the experimental results with theory showed good agreement in the prediction of a traveling-wave-type flutter, the flutter speed, and the wavelength. However, there was rather poor agreement in the prediction of the wave speed and frequency at flutter. Outside of the general difficulty of predicting the wave speed and frequency as accurately as the flutter speed, this discrepancy was attributed possibly to limitations in the experiment arising from a static depression at the leading edge of the panel, the cavity effect of the still air on the bottom side of the panel, buffeting at the trailing edge, and boundary layer effects.

Further work remains to be done to understand this problem area more fully. More careful experiments, better agreement in wave speeds and frequencies, experimental verification of the interesting relationship of divergence, flutter, and internal damping, the effects of still-air cavities, and the effects of boundary layers all need to be done yet. The related problem of subsonic flutter of panels without elastic foundations is also of interest. Some interesting work has been done by Greenspon and Goldman,[9] and again the existence of experimental subsonic flutter was revealed. These subsonic investigations should be of interest in the problems of hydroelastic panel flutter, axially symmetric cylinder flutter at low speeds, and panel flutter of inflatable structures at low speeds.

The extension of this work to the supersonic flutter of panels on continuous elastic foundations also would be of interest. Here again, Miles' infinite panel theory[1] can be used as a reference, and the effects of a finite panel, internal damping, etc., again can be investigated and compared with experiment. Miles' subsequent work on supersonic flutter of shells[10, 11] would be pertinent here.

Appendix: Influence of Still Air on Bottom Side of Panel

Using Miles' coordinate system as discussed in Sec. 3b, the additional pressure on the bottom side is

$$\Delta p = \rho_\infty(2\pi/\lambda)(c + U)^2 w_0 e^{i(ct-x)2\pi/\lambda} \tag{A1}$$

Adding the foregoing to the pressure for the top side and nondimensionalizing as before leads to the equation

$$(\zeta + 1)^2 - \zeta_0^2 + \mu(2\zeta^2 + 2\zeta + 1) = 0 \tag{A2}$$

Solving for ζ, one now obtains

$$c + U = [1/(1 + 2\mu)]\{\mu U \pm [(1 + 2\mu)c_0^2 - \mu(1 + \mu)U^2]^{1/2}\} \tag{A3}$$

The criterion for instability now becomes

$$U/c_0 > [(1 + 2\mu)/\mu(1 + \mu)]^{1/2} \tag{A4}$$

This criterion is indicated in Fig. 7 by the dashed line. For $\mu < 0.3$, this new criterion is the same as the previous one of Eq. (13). At higher values of μ, it approaches $2^{1/2}$ times the divergence criterion.

For the present panel, $\mu = 0.079$. Hence there is negligible change in the flutter speed and only a slight modification to the wave speed and frequency caused by this still air on the bottom. The divergence characteristics remain unaltered by the presence of this still air.

This analysis considered the still air to be large in depth. The effect of a small depth cavity on the pressure was not investigated. It is conceivable that it could give a greater influence on the flutter behavior. Acoustic or "organ-piping" resonance effects associated with a compressible gas also might be present here.

References

[1] Miles, J. W., "On the aerodynamic instability of thin panels," J. Aerospace Sci. **23**, 771–791 (1956).

[2] Dugundji, J., Dowell, E., and Perkin, B., "Subsonic flutter of panels on continuous elastic foundations—experiment and theory," Mass. Inst. Tech. Aeroelastic and Structures Research Lab. TR 74-4, Air Force Office Sci. Research (1962).

[3] Dowell, E., "The dynamic instability of panels on elastic supports in a supersonic flow," M.S. Thesis, Dept. Aeronaut. and Astronaut., Mass. Inst. Tech. (1961).

[4] Leonard, R. W. and Hedgepeth, J. M., "On panel flutter and divergence of infinitely long unstiffened and ring-stiffened thin-walled circular cylinders," NACA TR 1302, Langley Aeronaut. Lab., Langley Field, Va. (1957).

[5] Landahl, M. T., "On stability of an incompressible laminar boundary layer over a flexible surface," J. Fluid Mech. **13**, 609–632 (1962).

[6] Bisplinghoff, R. L., Ashley, H., and Halfman, R. L., *Aeroelasticity* (Addison-Wesley Publishing Co., Inc., Cambridge, Mass., 1955), Chap. V, pp. 285–326.

[7] Flax, A. H., "Aero- and hydro-elasticity," *Structural Mechanics, Proceedings of the First Symposium on Naval Structural Mechanics* (Pergamon Press, New York, 1960).

[8] Miles, J. W., "On panel flutter in the presence of a boundary layer," J. Aerospace Sci. **26**, 81–93 (1959).

[9] Greenspon, J. E. and Goldman, R. L., "Flutter of thin panels at subsonic and supersonic speeds," OSR TN 57-65, ASTIA 136, 560, Martin Co., Dynamics Research Staff (1957).

[10] Miles, J. W., "Supersonic flutter of a cylindrical shell," J. Aerospace Sci. **24**, 107–118 (1957).

[11] Miles, J. W., "Supersonic flutter of a cylindrical shell—II," J. Aerospace Sci. **25**, 312–316 (1958).